Pentacene-based organic field-effect transistors

2008 J. Phys.: Condens. Matter 20 184011

(http://iopscience.iop.org/0953-8984/20/18/184011)

J. Phys.: Condens. Matter **20** (2008) 184011 (16pp) doi:10.1088/0953-8984/20/18/184011

Pentacene-based organic field-effect transistors

Masatoshi Kitamura[1] **and Yasuhiko Arakawa**[1,2]

[1] Institute for Nano Quantum Information Electronics, University of Tokyo, 4-6-1 Komaba, Meguro-ku, Tokyo 153-8505, Japan
[2] Research Center for Advanced Science and Technology, University of Tokyo, 4-6-1 Komaba, Meguro-ku, Tokyo 153-8904, Japan

E-mail: kita@iis.u-tokyo.ac.jp

Received 4 September 2007, in final form 24 October 2007
Published 17 April 2008
Online at stacks.iop.org/JPhysCM/20/184011

Abstract
Organic field-effect transistors (FETs) have attracted considerable attention because of their potential for realizing large-area, mechanically flexible, lightweight and low-cost devices. Pentacene, which is a promising material for organic FETs, has been intensely studied. This article reviews the basic properties of pentacene films and crystals, and the characteristics of pentacene FETs fabricated under various conditions, including our recent achievement of low-voltage operating high-mobility FETs. The basic properties include the crystal polymorph, the band structure and the effective mass. These data have been used for discussion of carrier transport and mobility in pentacene films. The characteristics of pentacene FETs generally depend on the conditions of the pentacene film and the gate-dielectric surface. The dependences are summarized in the article. In addition, liquid-crystal displays and organic light-emitting device arrays using pentacene FETs are reviewed as applications of organic FETs, and complementary metal–oxide–semiconductor circuits using our low-voltage operating FETs are also shown.

(Some figures in this article are in colour only in the electronic version)

1. Introduction

Field-effect transistor (FET) technologies have been progressing since their discovery and have served as the foundations for the electronic and information industries. Most transistors are made of single-crystal, polycrystalline or amorphous silicon. Single-crystal-silicon FETs are mainly used for large-scale integrated circuits. The size of the silicon wafer has increased up to 300 mm in diameter to raise productivity and the transistor size has decreased to 65 nm in channel length for high speed and low power consumption. On the other hand, amorphous and polycrystalline silicon transistors are used as addressing devices for active matrix liquid crystal displays (LCDs). The glass-substrate size for LCDs with amorphous silicon thin-film transistors (TFTs) has increased to more than 2 m $\times$ 2 m. Despite this engineering progress, organic FETs have attracted considerable attention. This is because organic FETs have the attractive potential to realize large-area, mechanically flexible, lightweight and low-cost devices.

This potential mainly arises from a deposition process which can be adapted to various substrates, including glass and plastic substrates, since the organic materials for the channels of organic FETs can be deposited on the substrate at room temperature or relatively low temperatures. In addition, some soluble organic materials are available for deposition from the solution. This advantage allows deposition processes which do not require a vacuum stage, such as spin coating and ink-jet printing, to be used. Another advantage is that organic FETs with some materials have field-effect mobilities comparable to or higher than those of amorphous silicon TFTs. Obtaining a high mobility is important for device applications. This is because the output current and cut-off frequency are proportional to the mobility.

Many organic materials of small molecules and polymers have been used as channel materials for organic FETs. We can see many of these materials in review articles about organic transistors [1–3]. The organic materials have π orbitals, which play primary roles in the semiconductor properties and carrier transport. Not all the materials have superior properties and high mobility. Pentacene, which is an aromatic hydrocarbon and is shown in figure 1, is one of the promising materials with high mobility and has been widely and intensively studied.

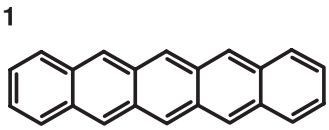

Figure 1. The molecular structure of pentacene. The upper-left figure **1** shows labels to identify the chemicals shown in this article.

More than 1000 articles related to pentacene transistors have been reported in scientific journals confirming its considerable importance [4].

Bailey and Madoff reported high yield synthesis of pentacene in 1953 [5]. In the literature, they commented that Clar and John had first synthesized pentacene from *m*-xylophenone [6]. Nowadays we can obtain pentacene from some chemical companies. This ready availability is another reason for the extensive research into pentacene transistors.

The field-effect mobilities of pentacene FETs with relatively high mobilities are plotted in figure 2. Pentacene FETs usually operate as p-channel (hole transporting) transistors. In 1991 Horowitz *et al* reported pentacene TFTs with a mobility of 0.002 $cm^2\ V^{-1}\ s^{-1}$ [7]. The TFT was fabricated on a doped silicon substrate serving as a gate electrode. Thermal silicon oxide was used as a gate insulator, and a metal for the source/drain electrodes was deposited on the pentacene film. The same configuration with a bottom gate and top source/drain electrodes has been used in many cases. The mobility of pentacene FETs dramatically increased in 1996–1997 [8–12]. In particular, Lin *et al* demonstrated a mobility of 1.5 $cm^2\ V^{-1}\ s^{-1}$ [12]. This high mobility is mainly attributed to surface treatment for the gate dielectric. This report has affected progress in organic transistor research. Many pentacene FETs with high mobilities of more than 1 $cm^2\ V^{-1}\ s^{-1}$ have been demonstrated since then and the mobility has been gradually increasing after that dramatic improvement. Pentacene FETs with mobilities of 3.0 [13], 3.3 [14] and 5.5 $cm^2\ V^{-1}\ s^{-1}$ [15] were reported in 2002, 2003 and 2006, respectively.

Many studies of pentacene FETs have been reported, as stated above. The subjects in the reports include device physics, growth, crystallography, electronic transport, dielectrics, surface science and device applications. A methodical review of the many reports will contribute to further progression for pentacene FETs, and also for FETs with other known and novel materials. The purpose of this article is to review studies of pentacene films and pentacene FETs, including our work. In particular, we have focused on useful information for the fabrication of high-performance pentacene FETs and for further improvement of their properties. In addition, some applications of pentacene TFTs are also reviewed to show the possibilities of organic transistors.

2. Metal–oxide–semiconductor FET

Useful equations for the evaluation and analysis of organic FET characteristics are summarized in this section. Organic FETs generally exhibit the same behaviour as silicon metal-oxide–semiconductor (MOS) FETs. Therefore, standard equations for

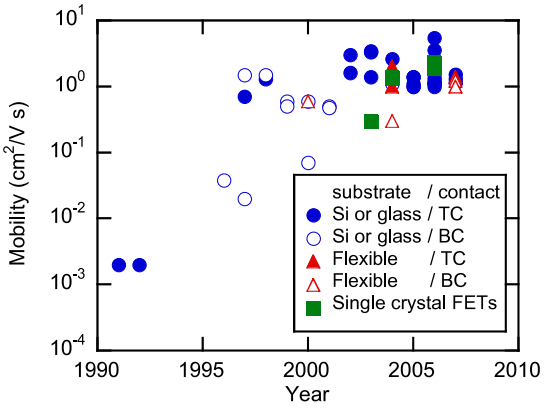

Figure 2. Field-effect mobility of pentacene FETs with high mobilities versus the year. Plotted mobilities are classified into structural types; the classification is shown in the inset. Abbreviations BC and TC denote bottom and top drain/source contacts, respectively.

silicon MOSFETs can be used for the purpose. In the gradual channel approximation, the drain current through channel material is represented by

$$I_D = \frac{W}{L}\mu C_{OX}\left[(V_G - V_{TH})V_D - \frac{V_D^2}{2}\right], \quad \text{for } |V_G - V_{TH}| > V_D \quad \text{(linear regime)}, \tag{1}$$

$$I_D = \frac{W}{2L}\mu C_{OX}(V_G - V_{TH})^2, \quad \text{for } |V_G - V_{TH}| < V_D \quad \text{(saturation regime)}, \tag{2}$$

where μ is the field-effect mobility, W and L the channel width and length, C_{OX} the gate capacitance per unit area, V_{TH} the threshold voltage and V_G and V_D the source–gate and source–drain voltages. The mobility in the linear regime is extracted from (1), and the mobility in the saturation regime and the threshold voltage are calculated by fitting to a measured $|I_D|^{1/2} - V_G$ curve with (2).

In many cases, organic transistors operate in the accumulation mode. The threshold voltage for an accumulation mode MOSFET equals a flat band voltage and can be written as

$$V_{TH} = (\Phi_M - \Phi_S) - \frac{1}{C_{OX}}\left(Q_S + \int_0^t \frac{x}{t}\rho_{OX}(x)\,dx\right). \tag{3}$$

Here Φ_M and Φ_S are work functions of the gate metal and the semiconductor, Q_S is the surface charge density at the interface between dielectric and the semiconductor and $\rho_{OX}(x)$ is the charge density per unit volume in the gate dielectric. The interfaces of the dielectric for the gate metal and the semiconductor are $x = 0$ and t, respectively. Subthreshold swing S is represented as

$$S = 2.3\frac{kT}{q}\left(1 + \frac{C_S}{C_{OX}}\right), \tag{4}$$

where $C_S = \varepsilon_S/x_S$ and x_S is the maximum depletion layer thickness. Equation (4) is given for inversion mode FETs. For accumulation mode FETs, subthreshold swing is expressed in a similar expression [16]. For both modes, the minimum value of S at room temperature is calculated to be about 60 mV/decade.

3. Pentacene thin-film and crystal preparations

3.1. Purification

The performance of organic FETs, as well as silicon-based FETs, depends on impurities. Even mobilities of silicon single crystal FETs drastically decrease with increasing impurity concentration. For a doping density of 10^{-19} cm^{-3}, which corresponds to a concentration of 0.02%, the electron mobility is less than 100 cm^2 V^{-1} s^{-1} [17]. Therefore, purification of organic source materials for active layers is important to obtain a high-performance transistor. Pentacene can be obtained from some chemical companies. In some cases, as-received pentacene requires further purification before use. In reality, a pentacene transistor fabricated from a freshly purified pentacene source has exhibited a higher mobility than one fabricated from a stored pentacene source [18].

Pentacene sources can be purified by train sublimation, which has also been used to obtain pentacene single crystals [19, 20]. Hydrogen mixed nitrogen and argon gases are used as flowing gases. Use of a low hydrogen concentration or low-purity gas leads to the production of impurities such as pentacenequinone. As a low-purity source is purified, black low-density residuals may remain at the position that the pentacene source is set.

For vacuum deposition, the deposition process itself can purify the source materials. This is because impurities with a lower sublimation temperature (higher vapour pressure) are removed from the source by heating below the sublimation temperature of the target material and impurities with a higher sublimation temperature (lower vapour pressure) remain in the source during the sublimation of the target material. For a solution process, source materials should be adequately purified before use because no such purification occurs.

3.2. Vapour pressure and vacuum deposition

For an organic material to be available for thermal deposition it is necessary that the material does not decompose up to the sublimation or vapour temperature. Pentacene is available for thermal deposition under high and low vacuum pressures. The vapour pressure and deposition rate of pentacene are described in this subsection. The data will be useful for achieving a controlled deposition rate of pentacene.

The vapour pressure of pentacene at various temperatures has been reported [21, 22]. Figure 3 shows the relation between the vapour pressure and the temperature. The measured vapour pressures of pentacene are fitted to the equation

$$\ln(p/p_0) = A - \Delta H/RT, \tag{5}$$

where A is a constant, ΔH a constant enthalpy of sublimation, R the gas constant and p_0 is a standard pressure (1 Pa). This equation is the integrated form of the Clausius–Clapeyron equation with a constant enthalpy of vaporization. In figure 3, the fitting line was obtained by substituting $A = 35.823$ and $\Delta H = 156.9$ kJ mol^{-1}. Using (5), the pressure at room temperature ($T = 300$ K) is of the order of 10^{-12} Pa. This shows that pentacene molecules mostly do not vaporize at room temperature at atmospheric pressure nor in high vacuum. For example, the pressures at $T = 170$ and 260 °C are calculated to be about 10^{-3} and 1.5 Pa, respectively.

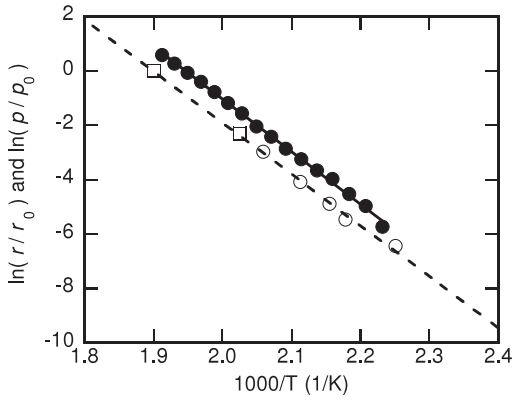

Figure 3. Vapour pressures and deposition rates of pentacene. Open squares and open circles denote vapour pressures reported in [21] and [22], respectively. Closed circles show deposition rates of pentacene in our deposition system.

Pentacene films deposited from the vapour phase have been provided by conventional thermal deposition, cluster beam deposition [23], pulsed laser deposition [24], molecular beam deposition in ultra-high vacuum [8] and physical vapour deposition (PVD) in a low vacuum [18]. Conventional thermal deposition is used for pentacene film deposition in many cases.

We use a thermal deposition system with crucibles for organic materials. The background pressure in the deposition system is of the order of 10^{-5} Pa. The deposition rate of pentacene is measured with an oscillating quartz thickness monitor during the deposition. The deposition rate is determined by the temperature of the crucible, while the relation between the rate and the temperature slightly changes depending on the amount of pentacene source in the crucible. The change for a source with impurities is larger than that for a high-purity source. The relation between the deposition rate and the crucible temperature is shown in figure 3 with the vapour pressure of pentacene. The experimental data are fitted to the equation

$$\ln(r/r_0) = B - C/T, \tag{6}$$

where r_0 is a reference rate equal to 1 Å s^{-1}, with B and C being constants. Evaluated values of B and C are 37.466 and 19 257. The value of $\Delta H/R$ for the vapour pressure in figure 3 is 18 870, which is close to the value of C. This indicates that the deposition rate is almost proportional to the vapour pressure. This result is consistent with a relation between the evaporation rate of molecules per unit area r_e and vapour pressure p,

$$r_e = p/\sqrt{2\pi mkT}, \tag{7}$$

where m is the molecule mass and k is Boltzmann's constant. The consistency shows that the relation (7) is valid for actual evaporation of pentacene molecules. This fact is useful for the estimation of deposition rate for other deposition systems.

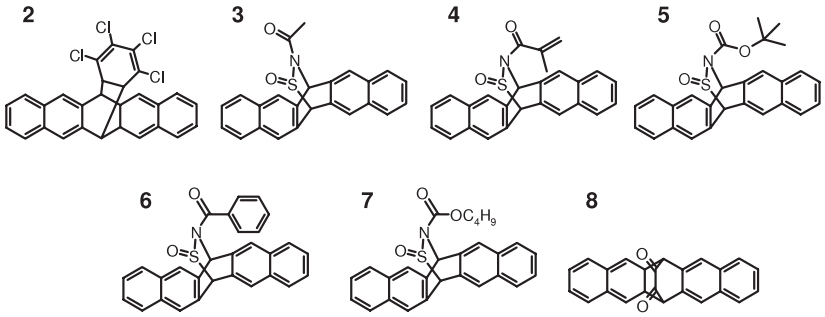

Figure 4. Molecular structures of precursors converting to pentacene.

Table 1. Mobility and process condition for pentacene transistors from solution processes.

Reference	Chemical	Mobility ($cm^2\ V^{-1}\ s^{-1}$)	Solution	Conversion conditions
[25]	2	0.009	0.5 wt% in dichloromethane	140–180 °C, 5 min to 2 h
[26]	2	0.2	1.5 wt% in dichloromethane	200 °C, 5 s
[27]	3	0.89	1–2% in chloroform	200 °C, 1.5 min
[28]	4	0.021	20 mg ml^{-1} in chloroform	UV irradiation, 150 °C, 5 min
[29]	5	0.25	In chloroform with PAG[a]	UV irradiation, 130 °C, 5 min
[30]	6	0.05	1 wt% in chloroform	160 °C, 5 min
[31]	7	0.068	20 mg ml^{-1} in PGMEA[b]/2-propanol (10:90%)	120 °C, 20 h
[32]	8	—	In toluene	UV irradiation, room temp.
[34]	1	0.45	0.1–0.3 wt% in trichlorobenzene of 60–180 °C	—

[a] PAG, photoacid-generating compound (di-*tert*-butyl-phenyliodonium perfluorobutanesulfonate).
[b] PGMEA, propylene glycol methyl ether acetate.

3.3. Solution process

An advantage of organic transistors is that the organic active layer can be prepared from a solution process. In many cases pentacene layers are deposited by thermal evaporation as described in the preceding subsection. On the other hand, a solution process is also available for pentacene layers, though there are fewer reports than that for thermal deposition. In general, soluble precursors to pentacene are used for the solution process [25–32] since pentacene is virtually insoluble in any solvent at room temperature. The molecular structures of the precursors are shown in figure 4. The precursors are converted to pentacene by heating and in some cases by irradiation with UV light. Transistor operation of pentacene FETs fabricated by the solution processes has been achieved with the exception of chemical **8**. The mobilities of the FET and the conversion conditions are summarized in table 1. The highest mobility of 0.89 was obtained from the FET with pentacene converted from chemical **3**.

Although pentacene has low solubility, it is soluble in heated trichlorobenzene. The solvent has been used for growth of single-crystal pentacene [33]. Minakata and Natsume have demonstrated pentacene FETs with an active layer coated from pentacene solution in 1,2,4-trichlorobenzene [34]. The mobility is higher than that for the precursors except for chemical **3**. Direct coating from pentacene solution has the advantage that the method does not require chemical reactions by heating or UV irradiation.

3.4. Single crystal

Pentacene single-crystal FETs are worth noting since carrier transport in the single crystal is not influenced by structural defects such as gain boundaries in polycrystalline films. Single crystals of pentacene are grown from the vapour or liquid phase. FETs with single-crystal pentacene grown from vapour have been reported [35–38]. The FETs exhibited field-effect mobilities of 0.30 [35], 1.4 [36], 1.9 [37] and 2.3 $cm^2\ V^{-1}\ s^{-1}$ [38]. Despite using single crystal as a channel material, these values are not high in comparison with pentacene TFTs shown later. The reason for this may be due to undesirable structural imperfections and impurities in the crystal, and/or intrinsic mobility of single-crystal pentacene. The latter presumption is based on effective masses calculated for pentacene crystals with different polymorphs.

4. Crystal phase, band structure and carrier transport

4.1. Crystal phase

To identify crystal structure is necessary to calculate the band structure and investigate carrier transport in the crystal. Crystal structures of single-crystal and thin-film pentacene have been reported. The lattice parameters of the crystals reported are summarized in table 2. The crystal structures can be classified into at least four polymorphs. The four polymorphs

Table 2. Lattice parameters of single-crystal and thin-film pentacene.

Polymorph	Reference	Pentacene[b] (Substrate)	a (Å)	b (Å)	c (Å)	α (deg)	β (deg)	γ (deg)	d_{001} (Å)
I	[41][a]	SC	6.28	7.71	14.44	76.75	88.01	84.52	14.1
	[45]	TF (Kapton)	—	—	—	—	—	—	14.1
II	[39][a]	SC	7.9	6.06	16.01	101.9	112.6	85.8	14.5
	[47]	TF (SiO_2)	7.9	6.08	15.84	101.3	112.7	85.7	14.4
III	[46]	TF(NaCl)	6.1	7.6	15.3	81	85	89.5	15.1
	[45]	TF (Kapton)	—	—	—	—	—	—	15.0
IV	[53]	TF (SiO_2)	7.5	5.92	15.35	90	90	91	15.4
	[48][a]	TF (SiO_2)	7.54	5.94	—	—	—	89.5	15.4

[a] Lattice parameters in [40, 42–44] for I, [40] for II and [49–51] for IV are almost the same as those in this row.
[b] SC and TF denote single crystal and thin film.

are labelled I–IV. The pentacene crystals are triclinic with herringbone packing of two molecules in a unit cell, though polymorph IV may have higher symmetry. The polymorphs are characterized by interplanar spacings between *ab* planes d_{001}, which are 14.1 Å for I, 14.5 Å for II, 15.1 Å for III and 15.4 Å for IV. Characterization by the spacing d_{001} is useful for thin films deposited on substrates. This is because the *ab* plane is parallel to the substrate surface and the spacing is easily measured by ω–2θ scan in x-ray diffraction (XRD) measurements. The spacing d_{001} is represented using axial lengths and angels as follows:

$$d_{001} = \left[1 - (\cos^2\alpha - 2\cos\alpha\cos\beta\cos\gamma + \cos^2\beta)/\sin^2\gamma\right]^{1/2}. \quad (8)$$

Single crystals of pentacene reported have $d_{001} = 14.1$ or 14.5 Å. Campbell *et al* investigated single-crystal pentacene crystallized from trichlorobenzene solution in detail using XRD measurement and reported the crystal structure in 1960 and 1961 [33, 39]. They showed the lattice parameters of the unit cell and also the positions of the carbon atoms. Two pentacene molecules in the unit cell were completely planar. The angle formed by two molecules in the unit cell was about 52.6° [39]. The crystal with $d_{001} = 14.5$ Å is classified as polymorph II. Single-crystal pentacene with the same lattice parameters was grown by fast sublimation in a N_2 atmosphere [40]. On the other hand, another crystal structure with $d_{001} = 1.41$ nm has been reported. The pentacene crystals were grown from trichlorobenzene solution [41, 42] and vapour [43]. As-received pentacene from a chemical company also had the same lattice parameters [40, 44].

For thin-film pentacene deposited on substrates, many reports show that the pentacene film had $d_{001} = 14.5$ or 15.4 Å. Exceptions are pentacene films with $d_{001} = 14.1$ or 15.1 Å deposited on polyimide [45], and with $d_{001} = 15.1$ Å deposited on NaCl [46]. All pentacene films deposited on SiO_2 reported are classified into polymorph II with $d_{001} = 14.5$ Å or IV with $d_{001} = 15.4$ Å.

Grazing incidence x-ray diffractometry (GIXD) [47–51] and electron diffraction [52] have been used to obtain lattice axes and angles for the crystal structure of pentacene thin films. Yoshida *et al* measured the lattice parameters of 50 nm thick pentacene films deposited on SiO_2 by GIXD [47]. As a result, they identified the crystal structure of the pentacene film with $d_{001} = 14.4$ Å as that of a single crystal of polymorph II measured by Campbell [39]. The pentacene film with $d_{001} = 14.4$ Å resulted from post-annealing or dipping in solvent of pentacene film with $d_{001} = 15.4$ Å. Doi *et al* obtained the lattice parameters of 50 nm-thick pentacene films with $d_{001} = 15.4$ Å though they showed no experimental XRD data [53]. The structure had lattice angles of $\alpha = 90°$, $\beta = 90°$ and $\gamma = 91°$. If the α and β exactly equal 90°, the crystal structure is not triclinic but is monoclinic.

Kakudate *et al* measured d_{001}, a, b and γ of pentacene films by GIXD and investigated the deposition temperature and thickness dependence of the crystal structure [48]. The obtained lattice parameters corresponded to those of polymorph II or IV. Pentacene films with thicknesses of less than 20 nm consisted of only polycrystals with polymorph IV. Pentacene films with thicknesses of more than 20 nm led to crystals with polymorph II. The concentration of polymorph II increased with the thickness of pentacene films. Pentacene films deposited at a higher temperature of 50 °C had a higher concentration of polymorph II than those for room-temperature deposition. Ruiz *et al* confirmed a similar thickness dependence for pentacene deposited on UV-ozone treated SiO_2 [49]. Polymorph IV was also observed from one-monolayer thick pentacene on amorphous SiO_2 [50] and 60 nm thick pentacene on surface-treated SiO_2 [51].

Polymorphs I and II have been referred to as the *single-crystal phase* or *bulk phase* in some articles. This is because single crystals of pentacene can be classified into polymorphs I or II. However, thin films of pentacene deposited at certain conditions are also classified as polymorph II. Thus, to avoid the duplicated classification, polymorphs I and II are referred to as the *single-crystal phase* and the *bulk phase*, respectively. On the other hand, polymorphs III and IV have been referred to as the *thin-film phase*. Polymorph III has been observed only under specific conditions, so that only polymorph IV is referred to as the *thin-film phase* in this article.

4.2. Band structure and effective mass

Understanding carrier transport in a semiconductor requires knowledge of the band structure of the semiconductor. The effective mass for a semiconductor, m^*, is defined as

$$\frac{1}{m^*} = \frac{1}{\hbar^2}\frac{\partial^2 E(\boldsymbol{k})}{\partial \boldsymbol{k}^2}, \quad (9)$$

Table 3. Bandwidths and effective masses for pentacene crystal of polymorph I, II and IV.

Polymorph	Reference	Method	VBW (eV)	CBW (eV)	m_h^*/m_0 [b]	m_e^*/m_0 [b]
I	[54]	TB	0.608[a]	0.588[a]	(1.02)	(1.05)
	[55]	TB	0.738[a]	0.728[a]	(0.85)	(0.86)
	[56]	TB			3.92	
	[57]	DFT	0.540[a]	0.670[a]	(1.15)	(0.93)
	[59]	DFT	0.225	0.305	0.88 (1.38)	0.77 (1.02)
II	[56]	TB			2.56	
	[57]	DFT	0.360[a]	0.570[a]	(1.74)	(1.10)
	[58]	DFT	0.145	0.149	(2.13)	(2.07)
	[59]	DFT	0.151	0.229	2.28 (2.04)	1.30 (1.35)
	[53]	DFT	0.170	0.210	2.6 (1.82)	1.9 (1.47)
	[60]	DFT	0.360[a]	0.570[a]	(1.74)	(1.10)
IV	[53]	DFT	0.330	0.560	0.2 (0.61)	0.3 (1.03)
	[60]	DFT	0.690[a]	0.770[a]	(0.97)	(0.87)

[a] The bandwidths are mixing bands of HOMO (LUMO) and HOMO − 1 (LUMO + 1).
[b] The values in parentheses are approximations calculated from (10).

from the dispersion relation of the energy $E(\boldsymbol{k})$ and is an exact second-rank tensor. Carrier mobility μ is inversely proportional to m^*, as shown in the following subsection. Therefore, a light effective mass is desirable for high mobility. Effective mass can be roughly estimated from just the value of the bandwidth E_{BW} using

$$m^* = \frac{2\hbar^2}{a_{\mathrm{L}}^2 E_{\mathrm{BW}}}, \tag{10}$$

even if the exact energy dispersion relation is unknown. This assumes that dispersion relation is simply written as $E(k) = E_{\mathrm{BW}} \cos(a_{\mathrm{L}}k)/2$ where a_{L} is a lattice constant. If band mixing between the highest occupied molecular orbital (HOMO) and the HOMO − 1 (or lowest unoccupied molecular orbital (LUMO) and LUMO + 1) occurs, the right-hand side of (10) should be doubled.

The energy bands of pentacene crystals have been calculated by the tight-binding (TB) method [54–56] and density-functional theory (DFT) [53, 57–60]. Table 3 summarizes the bandwidth and effective mass. The values in parentheses for the effective mass column are approximations calculated from (10). Note that the bandwidths correspond to HOMO (LUMO) or a mixing band of HOMO and HOMO − 1 (or LUMO and LUMO + 1) depending on the report. In some of the reports, lattice parameters calculated or measured by the authors were used though the parameters are close to those shown in table 2.

For polymorph I (single-crystal phase), the HOMO bandwidth (HBW) and LUMO bandwidth (LBW) are in the ranges 540–738 and 588–670 meV, respectively. The effective masses calculated from (10) are $m_h^*/m_0 = 0.85$–1.38 and $m_e^*/m_0 = 0.86$–1.05 where m_0 is the free electron mass. Hummer *et al* calculated the effective masses from the band structures [59]. The masses are slightly less than the values of the approximations. Despite the rough approximation, the differences are not too large. Troisi *et al* also estimated effective masses from band structure calculated by the TB method [56]. However, the masses are extremely large in comparison to other values for polymorph I. The reason for the difference may be due to the difference in the adopted crystal structure and orientation of molecules in the crystal. Effective masses for holes and electrons are comparable for each calculation.

For polymorph II (bulk phase), the m_h^*/m_0 and m_e^*/m_0 are 1.74–2.13 and 1.10–2.07, respectively. The values for polymorph II are larger than those for polymorph I. For polymorph II, the effective mass of electrons is smaller than that of holes.

Band structures for polymorph IV have also been calculated [53, 60]. The effective masses calculated by Doi [53] are relatively small even when comparing effective masses of $m_h^*/m_0 = 0.55$ and $m_e^*/m_0 = 0.33$ for silicon crystal. On the other hands, effective masses approximated from the bandwidths by Doi are $m_h^*/m_0 = 0.61$ and $m_h^*/m_0 = 1.03\ m_0$. The values are close to the approximated masses for the bandwidths by Parisse *et al* [60].

The effective masses for polymorph IV (thin-film phase) are the smallest for the three polymorphs. Pentacene thin films are classified into bulk or thin-film phases. Therefore, we expect that TFTs with pentacene films of thin-film phase have higher field-effect mobilities than those of the bulk phase. Note that electron effective masses are not too large for all polymorphs. This suggests that n-channel FETs using pentacene as a channel material are possible.

4.3. Charge transport and mobility

Study of charge transport in a material is important for device physics. Electrons transporting in organic material are more or less coupled with phonons. Therefore, the electron–phonon interaction should be considered for understanding charge transport. The process of charge transport is classified into three regimes on the basis of the relation between localization energy E_{L} and electronic intermolecular interaction J [61]. The energy E_{L} is defined as the difference in the lattice energy of the charged and the neutral ground states. The regimes are (1) weak ($J \ll E_{\mathrm{L}}$), (2) intermediate ($J \approx E_{\mathrm{L}}$) and (3) strong ($J \gg E_{\mathrm{L}}$) interaction regimes.

For the weak interaction regime, a small polaron localized to a single molecule is formed by electron–phonon interaction. Thus, hopping of a polaron from a molecule to the next provides charge transport. Many studies of polarons formed in organic molecular crystals have been reported, e.g. [62, 63]. For actual pentacene crystals, Deng and Goddard have calculated carrier mobility from the diffusion coefficient using an incoherent hopping model and the Einstein relation [64]. The calculation model virtually represents polaron transport. The carrier mobility in pentacene crystal with polymorph I was calculated to be 6.5 $cm^2\ V^{-1}\ s^{-1}$. The calculation was performed for a single crystal of pentacene and not for polycrystalline pentacene. The calculated value of 6.5 $cm^2\ V^{-1}\ s^{-1}$ is not high in comparison with the highest field-effect mobility of 5.5 $cm^2\ V^{-1}\ s^{-1}$ for a pentacene TFT [15]. This may be because the calculation was performed for polymorph I and the calculation is based on incoherent hopping transport.

For intermediate intermolecular interactions, the polaron is delocalized over several molecules. Hultell and Stafström have investigated polaron dynamics in pentacene crystals [61]. They showed a transition from a nonadiabatic to an adiabatic polaronic drift with an increase in interaction strength. Also, it was shown that the mobility increases from 22 $cm^2\ V^{-1}\ s^{-1}$ at $J = 30$ meV to 130 $cm^2\ V^{-1}\ s^{-1}$ at 100 meV in the case of a localization energy $E_L = 97$ meV.

For the strong interaction regime, the lattice relaxation is neglected and the transport corresponds to that of a conventional inorganic semiconductor. In this regime, carrier mobility is written as

$$\mu = \frac{q\tau}{m^*}, \tag{11}$$

where τ is relaxation time, which relates to carrier scattering. If some causes of carrier scattering exist, the inverse of the effective relaxation time is the sum of the inverse of individual relaxation times for the causes. The relaxation time for silicon crystal FETs is mainly caused by ionized-impurity and lattice-vibration scattering. The latter type of scattering is dominant at room temperature. For example, when the doping density is 10^{17} cm^{-3}, the field-effect mobilities of electrons and holes are about 800 and 300 $cm^2\ V^{-1}\ s^{-1}$, respectively, at room temperature [65]. Although relaxation time for a semiconductor generally depends on the quality of the crystal, field-effect mobilities of pentacene crystal with polymorph IV are estimated from the effective masses to be 270 $cm^2\ V^{-1}\ s^{-1}$ for electrons and 150 $cm^2\ V^{-1}\ s^{-1}$ for holes under the assumption that the pentacene crystal has the same relaxation time as the silicon crystal. Although the assumption is apparently unreasonable, no experimental results that either negate or affirm the high mobility have been shown. Measured mobilities of pentacene TFTs are two orders less than the mobilities roughly estimated above. The experimental data do not negate the high mobilities for the pentacene crystal. This is because the pentacene films for TFTs have polycrystalline structure and probably have many scattering sites. The magnitude relation of the mobilities, which are 6.5 $cm^2\ V^{-1}\ s^{-1}$ for the hopping mode, 22–130 $cm^2\ V^{-1}\ s^{-1}$ for polaron transport in intermediate interaction and 150 $cm^2\ V^{-1}\ s^{-1}$ for band transport described above, is notable.

Actual pentacene thin films are polycrystalline with many grain boundaries. The boundaries cause field-effect mobility to decrease. Horowitz and Hajlaoui have suggested that mobility for organic FETs with polycrystalline organic layers is written in the form

$$\mu = \frac{q\langle v\rangle l}{8kT}\exp\left(-\frac{E_B}{kT}\right), \tag{12}$$

where $\langle v\rangle$, l and E_B are the electron mean velocity, grain size and barrier height at the boundary, respectively [66]. When $\langle v\rangle$ does not depend on T, μ has the maximal value at $T = E_B/k$, increases at $T < E_B/k$ and decreases at $T > E_B/k$. The value of μ is proportional to l and diverges to infinity as l increases to infinity. This indicates that (12) yields a discrepancy at large grain sizes.

Carlo *et al* have suggested another expression,

$$\mu = \mu_I\frac{1}{1 + n_G\beta_G\exp(E_B/kT)}, \tag{13}$$

where μ_I is the intrinsic mobility in the grains which depends on electric field, n_G is the number of grain boundaries in the channel and $\beta_G = l_G/L$ (L: channel length, l_G: effective grain boundary size) [67]. The μ in (13) increases to the intrinsic mobility as n_G decreases to zero. The increasing behaviour is feasible. On the other hand, μ increases monotonically with temperature. Although the temperature dependence of (12) is consistent with that of (13) at low temperatures of $T < E_B/k$, discrepancy in the temperature dependences occurs at high temperatures $< E_B/k$.

The temperature dependence of mobility for pentacene TFTs has been experimentally investigated. In some cases, the mobility increases with temperature [68–70]. On the other hand, Nelson *et al* have shown that the mobility around room temperature slightly decreases with increasing temperature. The difference in the temperature dependence may be due to a difference in properties of pentacene films [71]. The temperature dependence of the mobility includes influences of contact resistance. Note that contact resistance also depends on measurement temperature [72].

4.4. Energy level alignment

To investigate energy level alignment at the interface of organic and metal layers it is useful to consider the carrier injection from the metal layer into the organic layer. The energy level alignment for pentacene has been investigated by ultraviolet and x-ray photoelectron spectroscopy (UPS and XPS) [73–76]. Figure 5 shows a schematic diagram of the energy band at the metal/pentacene interface. An interface dipole E_Δ occurs at the interface. The energy barrier height E_{BH} is written as $E_{BH} = (E_{HOMO} - E_\Delta) - \Phi_M$, where Φ_M is work function of the metal. Accordingly, a negative E_Δ increases E_{BH}. E_Δ is roughly represented as $E_\Delta = -(\Phi_M - 3.5)/1.8$ from figure 4 in [75]. E_Δ decreases linearly with increasing Φ_M. Since the gradient of the relation is less than 1, use of a metal with a large work function suppresses E_{BH}.

Table 4. Energies for band alignment at interfaces between pentacene (Pen) and Au (or PEDOT/PSS).

Reference	Configuration	Φ_M (eV)	E_{HOMO} (eV)	Φ_S (eV)	E_Δ (eV)	E_{BH} (eV)
[73]	Pen on Au	4.65	4.80	4.2	−0.3	0.45
[73]	Pen on O_2–Au	5.28	4.72	4.32	−0.71	0.15
[74]	Pen on Au	5.4	5.2	4.35	−1.05	0.85
[74]	Pen on PEDOT/PSS	4.85	5.0	4.75	−0.1	0.25
[75]	Pen on Au	5.4	4.9		−1.0	0.5
[75]	Au on Pen	4.2	4.9		−0.3	1.0
[76]	Pen on Au	5.47	4.52		−0.95	0.55

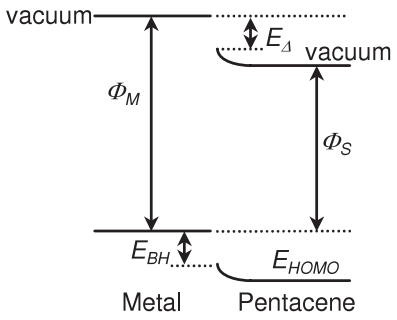

Figure 5. Energy diagram for the interface between pentacene and metal.

The experimentally obtained data are summarized in table 4. E_{BH} at the interface of pentacene on Au ranges from 0.45 to 0.85 eV. A reason for the large difference is due to the difference in the surface condition of the Au. Φ_M is actually in the range of 4.65–5.47 eV. Kim *et al* have investigated an O_2 plasma treatment for Au surface [73]. The treatment provides a O_2–Au surface with a high work function of 5.28 eV. As a result, E_{BH} decreases to 0.15 eV. The barrier height is the lowest in table 4. For pentacene on poly(3,4-ethylenedioxythiophene)/poly(styrenesulfonate) (PEDOT/PSS), E_Δ was −0.1 eV. The small E_Δ leads to small $E_{BH} = 0.25$ eV. The value of Φ_M of Au on pentacene was 4.2 eV. This value is so small that E_{BH} increases to 1.0 eV. Note that Φ_M of Au on pentacene probably depends on the deposition conditions.

5. Pentacene thin film

Pentacene thin films deposited by thermal evaporation are reviewed in this section. In particular we focus on the dependence of the grain size in the films on the deposition conditions. In general, pentacene growth on a substrate proceeds as follows. A molecule sublimating from the source adsorbs on the surface of a substrate and diffuses on the surface. As more than a critical number of molecules aggregate, the molecules form a two-dimensional (2D) island. The 2D island laterally grows, incorporating diffusing molecules. After deposition of one or some monolayer(s), the growth mode transforms to three-dimensional (3D) growth. The growth mode and morphology depend on deposition and surface conditions. The deposition conditions includes deposition rate, substrate temperature and kinetic energy of the sublimating molecules. The surface conditions depend on the material used, the surface treatment and surface roughness. Much knowledge of pentacene growth can be obtained from the review article by Ruiz *et al* [77].

Growth modes on substrates are generally classified into (1) layer-by-layer (Frank–van der Merwe), (2) layer followed by island (Stranski–Krastanov) and (3) island (Volmer–Weber) growth modes. The pentacene growth mentioned above corresponds to the Stranski–Krastanov mode. Low surface energy for growth material leads to the Volmer–Weber mode. Therefore, pentacene grown on a substrate with low surface energy, such as a substrate treated with octadecyltrichlorosilane (OTS), exhibits the Volmer–Weber mode rather than the Stranski–Krastanov mode in some cases.

We have investigated the influence of deposition rate on nucleation density for pentacene deposition. Figures 6(a)–(c) show AFM images of 1 nm thick pentacene deposited on a SiO_2 surface [78]. The deposition rates are (a) 0.12 nm min^{-1}, (b) 1.2 nm min^{-1} and (c) 12 nm min^{-1}. For all deposition rates 2D islands were observed. The density of the 2D island strongly depends on the deposition rate. Stadlober *et al* have shown a similar dependence for substrates of SiO_2, polymethylmethacrylate (PMMA) and poly-4-vinylphenol (PVP) [79]. They suggested that the relation between deposition rate r and nucleation density N_{sat} is written as

$$N_{sat} \propto \left(\frac{r}{D}\right)^p \exp\left(\frac{E_N}{kT_s}\right), \tag{14}$$

where D is the diffusion coefficient of molecules, $p = i/(i+1)$, i is the critical island size, $E_N = (E_i + iE_D)/(i+2)$, E_i is nucleation energy, E_D is the activation energy of pentacene monomer diffusion and T_s is substrate temperature.

Figures 6(d)–(f) show AFM images of 60 nm thick pentacene deposited on a SiO_2 surface. The density of the 3D grains also depends on the deposition rate. Stadlober *et al* and Yagi *et al* have also confirmed the dependence for thick pentacene films [79, 80]. From a comparison of (a)–(c) and (d)–(f) in figure 6, the 3D grain density is less than that of the 2D island. This indicates that the 3D grain results from coalescence of small islands. On the other hand, Tejima *et al* have shown that the grain density does not depend on the nominal thickness of pentacene in the range of 11–46 nm [81]. This suggests that coalescence of 2D islands completes up to 11 nm. For 60 nm thick pentacene, a large grain is dendritic and valleys form in the large grain. This indicates that the structure reflects the coalescence of the 2D islands. Yang *et al* have investigated the growth process of pentacene from 1 monolayer (ML) to several ML in detail [82].

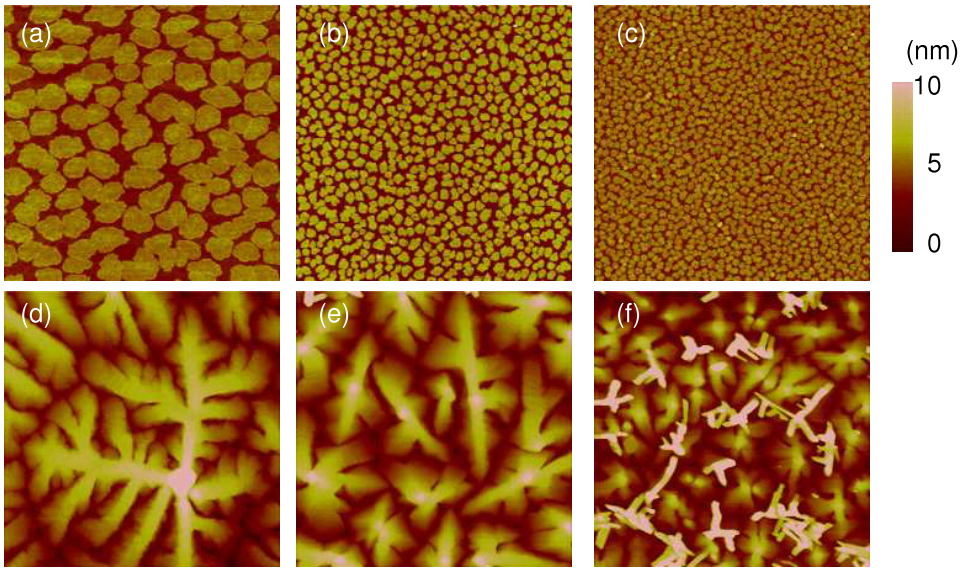

Figure 6. AFM images of pentacene deposited on a SiO_2 surface. The AFM image size is 5 μm × 5 μm. The deposition rates are (a) and (d) 0.12 nm min^{-1}, (b) and (e) 1.2 nm min^{-1}, and (c) and (f) 12 nm min^{-1}. The nominal thicknesses are (a)–(c) 1 nm and (d)–(f) 60 nm.

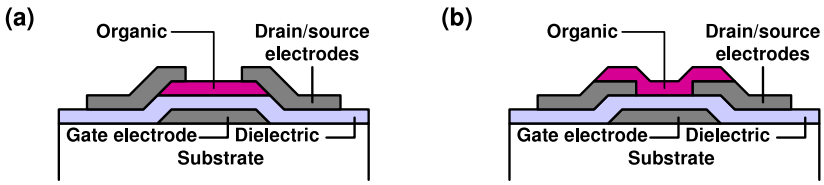

Figure 7. Schematics of organic TFTs: (a) top-contact configuration, (b) bottom-contact configuration.

Another principal parameter of pentacene growth is substrate temperature. In general, grain size increases with substrate temperature. Note that the crystal phase of pentacene film depends on substrate temperature. The ratio of the bulk phase to the thin-film phase increases with substrate temperature [83, 84]. On the other hand, the ratio of the bulk phase does not depend on deposition rate [83].

Grain size is also influenced by the surface roughness of substrates. The grain size decreases with increasing surface roughness using a substrate with a surface roughness of 0.11–0.25 nm. However, the substrate materials were different, and the surfaces had a different surface energy. Therefore, the dependence of the grain size probably includes the influence of the surface-energy difference. On the other hand, Steudel *et al* investigated the morphology of pentacene deposited on SiO_2 with different surface roughness. The results also showed that the grain size decreases with increasing surface roughness [85].

Dependence of grain size on surface energy has also been investigated. Yang *et al* achieved a polymer surface with different surface energies using poly(imide-siloxane) [82]. The pentacene deposited on the polymer with high surface energy had a large grain. In general, surfaces treated with organic chemicals have lower surface energy than inorganic surfaces. Pentacene grain size deposited on a SiO_2 surface treated with OTS is significantly smaller than that for an untreated surface [18, 83].

6. Pentacene thin-film transistors

6.1. Organic TFT structure

When designing organic TFTs, it should be remembered that the organic materials are often damaged by the fabrication process. The structure of organic TFTs is usually the top drain/source electrode structure of figure 7(a) or the bottom drain/source electrode structure of figure 7(b). For the top-contact configuration, electrodes are patterned with shadow masks in order to avoid damage to the organic layer. However, the use of shadow masks limits the channel length. Usually the channel length is of the order of 10 μm. On the other hand, the channel length is limited by the resolution of lithography for the bottom-contact configuration. A channel length of the order of 1 μm is possible at least.

Silicon single-crystal wafer is used as a substrate for convenience in many studies. Glass substrates are necessary for applications to LCD and organic light-emitting device (OLED) displays. Plastic substrates are also available since a high substrate temperature is not needed for pentacene deposition. Polyester (PET) [86], polyethylene naphthalate

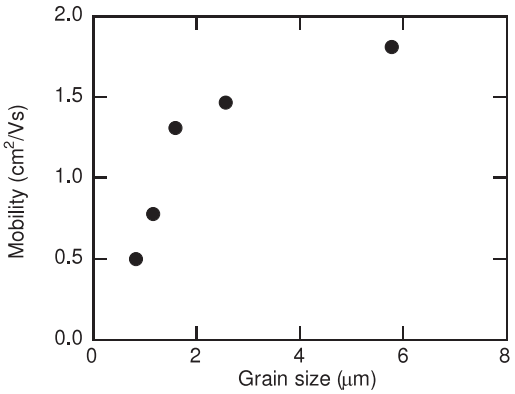

Figure 8. Relation of mobility of pentacene FETs and grain size.

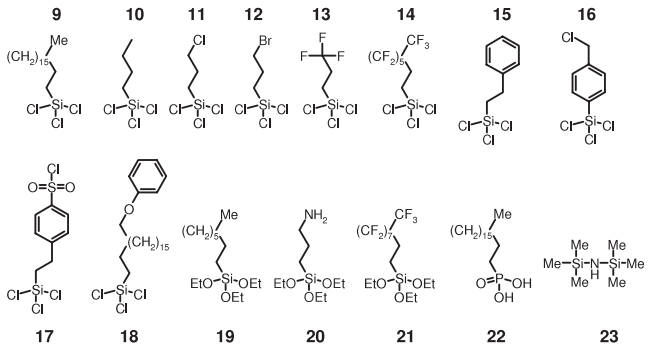

Figure 9. Chemicals used for surface treatment of gate dielectrics.

(PEN) [87], polyimide [88] and commercially available Mylar^{TM} films [89] have been used as substrates of pentacene TFTs.

When using a silicon substrate, the doped silicon serves as a gate electrode instead of a gate metal. On the other hand, a metal electrode is necessary for a glass or plastic substrate. Some metals such as Cr, Ti, Ta and Al, and indium–tin oxide have been used as gate electrodes. The metals may be selected on the basis of advantages in the fabrication process. Although the threshold voltage of a transistor depends on the work function of the gate electrode as in (3), the subject has not been investigated in detail.

6.2. Relation between grain size and mobility

Grain size in pentacene films significantly influences carrier transport in the films. We have investigated the relation between grain size and mobility of pentacene TFTs with SiO_2 dielectric [78]. Figure 8 shows the field-effect mobility of pentacene TFTs versus grain size. The pentacene films with different grain sizes were obtained by changing the deposition rate. The pentacene films with grain sizes of 5.8, 1.6 and 0.8 μm in figure 8 correspond to figures 6(d)–(f). The mobility increases monotonically with the grain size. This characteristic implies that further increase in grain size saturates the mobility. Carlo *et al* have observed a similar relation in saturated behaviour, though the mobility is less than those in figure 8 [67]. Knipp *et al* have shown that mobilities for pentacene deposited on SiO_2 and OTS-treated surfaces increases with the grain size [83]. On the other hand, a TFT with large-grain pentacene deposited on an OTS-treated surface at a high temperature had a lower mobility than that with small-grain pentacene deposited at a low temperature [18]. This may be because the pentacene films with different grain sizes were obtained by changing the substrate temperature.

The dependence shown in figure 8 seems to be consistent with (13). If the expression for the relation in (13) is appropriate, the mobility of 1.8 $cm^2\ V^{-1}\ s^{-1}$ for a grain size 5.8 μm is near to the intrinsic mobility for the pentacene single grain. However, many valleys exist in the large grain as mentioned in the preceding section. The valleys probably cause decreases in the mobility. Therefore, we need to know the substantial grain size rather than the apparent large grain size, and should use the substantial grain size for further consideration.

6.3. Surface treatment for gate dielectrics

Gate dielectric surfaces of organic FETs have been treated using various kinds of organic compound in order to improve the transistor performance. When Lin *et al* demonstrated high-mobility pentacene TFTs for the first time, they performed the surface treatment using OTS (**9** in figure 9) [12]. For improvement in mobility of FETs it is important to reduce trap and scattering states at the interface between the semiconductor and the dielectric. Surface treatment probably contributes to a decrease in such states that disturb carrier transport. Chemicals used for surface treatment of gate dielectrics are shown in figure 9. The chemicals are classified into (1) trichlorosilane (**9**–**18**) [83, 90, 91], (2) alkoxysilane (**19**–**21**) [92], (3) phosphonic acid (**22**) [14, 93] and (4) silazane (**23**) [94] according to the reaction group. Some of the chemicals have been used to obtain self-assembled monolayer (SAM). The surface treatment mainly influences the mobility, threshold voltage and subthreshold swing.

Knipp *et al* have compared the performances of pentacene TFTs on SiO_2 layers without and with OTS treatment [83]. Although the grain size for OTS treatment was smaller than that for no treatment, the mobility for OTS treatment was higher than that for no treatment. Pernstich *et al* used chemicals **9**–**17** and compared the transistor performance, in particular mobility and subthreshold swing [90]. The TFT with OTS treatment exhibited the highest mobility and the smallest subthreshold swing. Comparing results for chemicals **9** and **10** shows that the mobility for **9** with a long alkyl chain was higher than that for **10** with a short alkyl chain. This implies that the thickness of the organic layer formed by surface treatment influences mobility. On the other hand, hexamethyldisilazane (HMDS) (**23**) was effective for high mobility though the layer is much thinner than for **9** and **10**.

Surface treatment also influences the threshold voltage. Kobayashi *et al* have confirmed the shift using chemicals **19**–**21** with end groups of CF_3, CH_3 and NH_2 [92]. The chemicals with a CF_3 (NH_2) end group lead to a positive (negative) shift of threshold voltage. The positive shift of the CF_3 end group was also observed by Pernstich [90]. The threshold

Table 5. Pentacene TFT performance with various gate dielectrics.

Reference	Material	Dielectric constant	Mobility ($cm^2\ V^{-1}\ s^{-1}$)	C_{ox} ($nF\ cm^{-2}$)	Thickness (nm)	Voltage (V)
[12]	SiO_2 [a]		1.5		350	80
[83]	SiN_x		0.55			
[95]	Al_2O_3	9	0.6	24.1	330	60
[95]	$LaAlO_3$	15	1.4	40.2	330	40
[96]	Ta_2O_5		0.51			5
[97]	TiO_2 [a]		0.25	465		1
[98]	$Ti_{0.17}Si_{0.83}O_2/SiO_2$ [b]	15.8	1.16	192	73	5
[13]	PVP	3.6	3.0	11.4	280	30
[100]	PVA	3.3	1.1	326	9	2
[101]	Polyimide		1		540	100
[102]	Polymer bilayer	7.2	1	8.5	750	30
[103]	SiO_2/PMMA		1.4		128	30
[104]	SiO_2/polyimide		2.05			40
[105]	Ta_2O_5/PMMA		0.6		120	30
[106]	YO_x/PVP	7.6	1.74	70.8	95	5

[a] OTS was used for surface treatment.
[b] HMDS was used for surface treatment.

voltage shift may be caused by the existence of dipoles or extra charges induced by the treatment. Dipoles and charges in a gate dielectric are related to a flat band voltage by (3).

6.4. Gate dielectric

The condition of the gate dielectric as well as surface treatment has a large influences on transistor performance. In general, insulation and flatness are needed for gate dielectrics at least. Various materials have been used as gate dielectrics for organic FETs. The materials used are classified into (1) inorganic, (2) organic and (3) inorganic/organic hybrid materials. Table 5 shows the properties of pentacene TFTs with various kinds of gate dielectric layers. The TFTs with relatively high mobilities compared to other TFTs reported are summarized in the table.

For inorganic dielectrics, SiO_2, SiN_x [83], Al_2O_3 [95], $LaAlO_3$ [95], Ta_2O_5 [96], TiO_2 [97] single layers and a $Ti_{0.17}Si_{0.83}O_2/SiO_2$ [98] bilayer were used. In general, bandgaps of dielectrics decrease with the increasing dielectric constant [99]. Therefore, SiO_2 is the most promising material as a gate dielectric in term of insulation. In addition, use of SiO_2 enables the surface to be treated by chemicals shown in figure 9. On the other hand, gate materials with a high dielectric constant (high-k) provide high gate capacitance and contribute to a large output current, low threshold voltage and small subthreshold swing from (1) to (4). Gate dielectrics of Ta_2O_5 and TiO_2 were used to achieve low-voltage operation [96, 97]. However, large leakage current is of concern because of the small band gaps. High field-effect mobility comparable to that of TFTs with SiO_2 gate dielectric was achieved using $LaAlO_3$, though operational voltage was not low [95]. Probably the highest mobilities for TFTs are achieved when the pentacene layer is deposited directly on an inorganic dielectric surface. The fact is notable since a high field-effect mobility is generally obtained using TFTs with a surface-treated dielectric or organic dielectric.

Adopting a bilayer consisting of high-k material and SiO_2 allows low-voltage operation and surface treatment. We demonstrated low-voltage-operating high-performance pentacene TFTs using a bilayer consisting of a thick $Ti_{0.17}Si_{0.83}O_2$ layer and a thin SiO_2 layer [98]. The surface of the SiO_2 layer was treated by HMDS (**23**). The mixed metal oxide $Ti_{0.17}Si_{0.83}O_2$ had a flat surface comparable to thermal silicon oxide and the flatness contributed to the high field-effect mobility.

For organic dielectrics, PVP [13], polyvinyl alcohol (PVA) [100] and polyimide [101] single layers and a bilayer of terpolymer electret poly(vinylidene fluoride/tetrafluoroethylene/hexafluoropropylene) and polymer poly(vinyl cinnamate) [102] were used. All TFTs with the organic dielectrics exhibited field-effect mobilities of more than 1 $cm^2\ V^{-1}\ s^{-1}$ in contrast to the TFTs with inorganic dielectrics without surface treatment. The high mobility is attributed to the deposition of pentacene on the polymer surface. Actual pentacene TFTs with bilayers of SiO_2 and polymer had a high mobility [103, 104]. In general, the low dielectric constant of polymers causes a small gate capacitance and leads to high operational voltage and low output current. A solution to this problem is to use a thin-film gate dielectric [100]. The other is to adopt a bilayer consisting of high-k material and polymer [106]. Pentacene TFTs with a YO_x/PVP dielectric exhibited the highest mobility under operation at several voltages.

The results shown in this subsection confirm that adopting surface treatment or inserting a polymer layer is useful to achieve high mobility transistors.

6.5. Drain/source electrodes

For pentacene FETs, Au is mostly used for the drain and source electrodes. This is because Au has a relatively high work function compared to other metals. However, the work function depends on the surface condition, as described in section 4.4. The deposition conditions also affect the conductivities of Au, which increase with the deposition

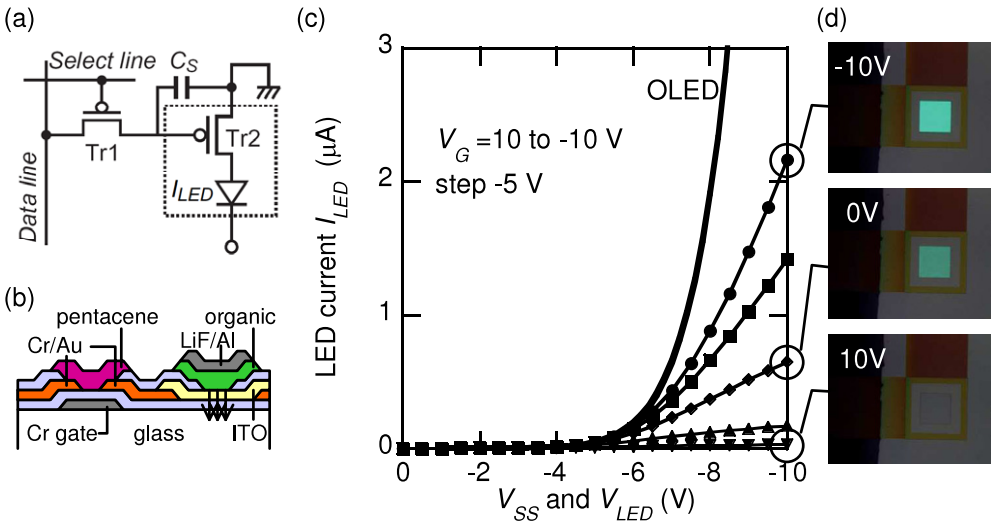

Figure 10. (a) A pixel circuit for an OLED display. (b) Schematic cross-section of an OLED driven by a pentacene TFT. The device corresponds to the circuit in the dotted line of (a). (c) Current characteristics through the OLED. The thick line shows the current of the OLED directly driven without a TFT. (d) Photographs of the OLED driven by the TFT at gate voltages of −10, 0 and 10 V.

rate [107]. This dependence influences the mobility of pentacene TFTs with Au top contact electrodes.

Charge injection is improved by inserting a metal oxide layer between pentacene and metal. Pentacene TFTs with a MoO_3/Al drain/source electrodes had higher mobility than with Au electrodes [108]. Insertion of an organic layer is also useful to reduce the contact resistance. Copper phthalocyanine (CuPc) has been used as the insertion layer [109]. For a bottom-contact configuration, treatments with 4-nitrobenzenthiol [110] and O_2 plasma [111] have been performed to improve charge injection.

There is another issue relevant to drain/source contact for the bottom-contact configuration. Usually an adhesion layer for contact between Au and the gate dielectric is used. Chromium and Ti have been used as the adhesion layer. However, thick adhesion layers cause increase the contact resistance. Yoneya *et al* have adopted a SAM prepared from 3-mercapto-propyl-trimethoxy silane as an adhesion layer instead of a metal [112]. They realized low contact resistance and high mobility for pentacene TFTs with bottom contacts.

7. Applications

7.1. Liquid crystal display

Thin-film transistors are mostly used for active matrix LCDs at present. Although current LCDs adopt amorphous or polycrystalline silicon TFTs as addressing devices, the use of organic TFTs for LCDs is a suitable application since organic transistors have the advantage of allowing flexible and lightweight displays. Some groups have reported LCDs with addressing pentacene TFTs [113–116]. The specification of the demonstrated LCDs has been increasing as summarized in table 6. Full-colour LCDs driven by pentacene TFTs have recently been demonstrated [116].

Difficulties in practical application are limitation of area for transistors and degradation by fabrication processes after deposition of the organic layer. The former require a bottom-contact configuration in order to fabricate transistors with a short channel length, which is typically about 5 μm. Adopting a bottom-contact structure leads to a large dependence of transistor characteristics on the adopted structure and fabrication process. Nomoto *et al* improved contact resistances of drain/source electrodes using a thin titanium adhesion layer [115]. On the other hand, Kawasaki *et al* investigated the influence of electrode structure on pentacene film morphology and reduced the contact resistance by adjusting the photolithography conditions for the electrodes [116]. For the latter, passivation over an organic layer is necessary for protection of the organic layer. Passivation layers used are shown in table 6. The passivation is useful for other applications.

7.2. Organic light-emitting devices

OLEDs are candidates as emitting devices for next-generation flat panel displays since OLEDs are self-emitting devices in contrast to liquid crystal cells. Organic layers for OLEDs are deposited by thermal evaporation or a solution process, and the fabrication process for OLEDs has similar advantages to that for organic transistors. Therefore, we can expect application of OLEDs to flexible and/or lightweight displays. For active matrix displays, two or more TFTs are used for 1 pixel in an OLED display. Although polycrystalline and amorphous silicon TFTs are generally used for the active matrix, organic TFTs are attractive because of their advantages. Organic TFTs will be applicable for use as the driving transistors of OLEDs since they have field-effect mobilities comparable to or more than those of amorphous silicon TFTs.

We demonstrated pentacene TFTs driving OLEDs in 2003 [117]. Figure 10 shows the current characteristics of a pixel with a pentacene TFT and an OLED. The luminance from the OLED was modulated by the applied gate voltage of the TFT. The OLED was of a practical size and showed

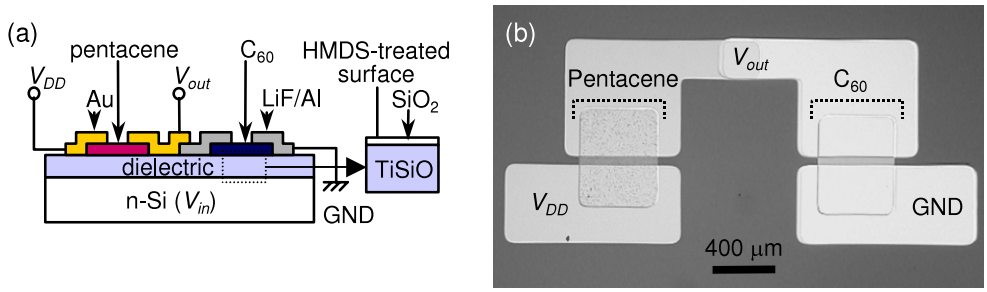

Figure 11. (a) Cross-section of an organic CMOS inverter with pentacene and C_{60} TFTs. (b) A photograph of an organic CMOS inverter.

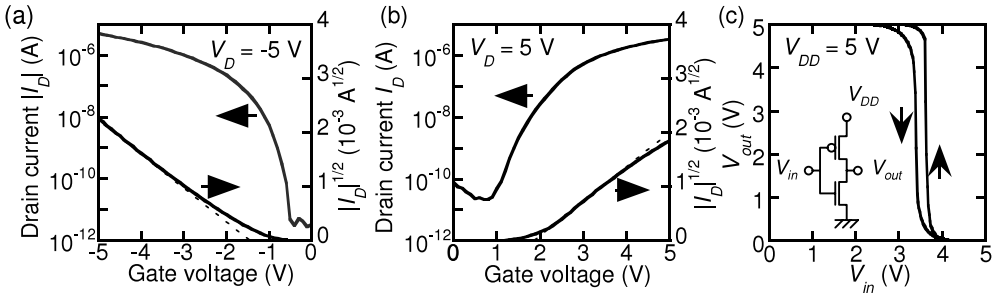

Figure 12. Transfer characteristics of (a) a pentacene TFT and (b) a C_{60} TFT. (c) Switching characteristic of an organic CMOS inverter.

Table 6. Demonstration of LCDs with pentacene TFTs as addressing transistors.

Reference	Year	Substrate	Pixel number	LC type[a]	Passivation
[113]	2001	PET	2 × 3	PD	SiN_x
[114]	2002	PEN	16 × 16	PD	PVA
[115]	2005	Glass	160 × 120	TN	SiN/PVA
[116]	2006	Glass	80 × 80 × 3 (RGB)	TN	PVA/glass resin

[a] PD and TN denote polymer-dispersed and twist-nematic, respectively.

luminance sufficient for practical applications. Pixel circuits for OLED displays require two transistors at least per pixel. The pixel circuit with two transistors is shown in figure 10. The transistor Tr1 operates to hold charges stored to the gate of transistor Tr2. We confirmed the function of two-transistor circuits using CuPc as an channel material [118], though no OLED was incorporated into the circuit.

OLED pixel arrays with organic TFTs as driving transistors have been reported [119–122]. Ohta *et al* [119] and Zhou *et al* [120], respectively, demonstrated 8 × 8 and 48 × 48 arrays on glass substrates. Recently, Zhou *et al* fabricated 48 × 48 OLED pixel arrays on a PET substrate [121] and Mizukami *et al* fabricated 16 × 16 OLED pixel arrays on a PEN substrate [122].

7.3. Complementary MOS circuits

Complementary MOS (CMOS) circuits are essential for digital circuits and contribute to low power consumption. The CMOS elements such as an inverter consist of p-channel and n-channel MOSFETs. Application of organic FETs to CMOS circuits expands the applications of CMOS circuits. Pentacene FETs are candidates as p-channel transistors for organic CMOS circuits because of their high performance.

A straightforward configuration of organic CMOS elements is to use a pentacene FET as the p-channel transistor and a high performance n-channel organic FET. n-channel organic transistors with high mobilities have been demonstrated using thiazole oligomer [123], perylene derivative [124] and C_{60} [125] as channel materials. We adopted a C_{60} transistor as an n-channel transistor for a CMOS inverter since the highest mobility of 6 $cm^2\ V^{-1}\ s^{-1}$ was achieved using C_{60} transistors [125].

An illustration and photograph of an organic CMOS inverter that we fabricated using pentacene and C_{60} FETs are shown in figure 11. The inverter was fabricated on a silicon substrate, which serves as a gate electrode. For low-voltage operation, we used a high-*k* material-based gate dielectric. The gate dielectric consisting of titanium–silicon oxide (TiSiO) and thin SiO_2 layers has a capacitance per unit area of 192 $nF\ cm^{-2}$. Figures 12(a) and (b) show the current–voltage characteristics of individual transistors. Both transistors operated at a voltage of 5 V. The low-voltage operation is attributed to the use of a gate dielectric with high capacitance. The field-effect mobilities and threshold voltages are 0.42 $cm^2\ V^{-1}\ s^{-1}$ and −1.5 V for the pentacene TFT and 0.45 $cm^2\ V^{-1}\ s^{-1}$ and 1.9 V for the C_{60} TFT, respectively.

From the measured threshold voltages, the inverter will operate at voltages of more than 3.4 V. The output characteristic of the inverter is shown in figure 12(c). Switching characteristics were observed at a voltage of 5 V as expected.

Use of glass substrates instead of silicon substrates is importance for useful applications. We have demonstrated CMOS inverters fabricated on glass substrates operating at voltages of 1–5 V [126]. Klauk *et al* have also achieved low-voltage operation of organic CMOS circuits using SAM gate dielectrics [93].

If p-channel and n-channel transistors are realized by use of a material, use of another organic material can be eliminated. We can expect that pentacene has electron transport properties judging from the conduction band dispersion and electron effective mass as mentioned in section 4.2. Ahles *et al* have demonstrated an n-channel pentacene transistor, inserting a Ca or PMMA layer between pentacene and the SiO_2 gate dielectric [127]. The mobilities are 0.10 $cm^2\ V^{-1}\ s^{-1}$ for the Ca interface layer and 0.12 $cm^2\ V^{-1}\ s^{-1}$ for the PMMA layer. They achieved inverter operation using pentacene transistors with a Ca layer and no interface layer.

Another way to construct CMOS elements is to use ambipolar transistors. Kang *et al* have fabricated ambipolar transistors using C_{60} and pentacene [128]. The ambipolar transistor consisted of SiO_2 dielectric, a pentacene lower layer and a C_{60} upper active layer, Au drain/source electrodes and a LiF overlayer covering the channel region. Current characteristics for ambipolar transistors were observed, though the measured field-effect mobilities were 0.017 $cm^2\ V^{-1}\ s^{-1}$ for p-channel and 0.007 $cm^2\ V^{-1}\ s^{-1}$ for n-channel operations, respectively. Ambipolar transistors have also been achieved using a single channel layer of pentacene [129]. Singh *et al* have demonstrated pentacene ambipolar transistors adopting PVA as a gate dielectric. The hole and electron mobilities were 0.3 and 0.04 $cm^2\ V^{-1}\ s^{-1}$, respectively.

The measured electron mobilities for pentacene range up to 0.12 $cm^2\ V^{-1}\ s^{-1}$ [129], which is less than those of n-channel FETs with other materials [123–126]. The electron mobility for pentacene will be improved by optimization of the fabrication processes and construction of transistors if the calculated effective masses for electrons are appropriate.

8. Prospect

We have reviewed many studies about pentacene films and FETs in this article. Many pentacene TFTs with field-effect mobilities of more than 1 $cm^2\ V^{-1}\ s^{-1}$ (comparable to those of amorphous silicon TFTs) have been achieved. This may indicate that amorphous silicon TFTs can be technologically replaced by pentacene TFTs. Although we can definitely expect that, some issues remain for actual applications. The area size for a transistor is limited, as mentioned in section 7.1, and operational frequency is specified for the applications. These require a bottom-contact configuration to suppress the area size and to form a short channel. Many pentacene TFTs with reported high mobilities have adopted the top-contact configuration. Therefore, more research for improvement in performance of TFTs with a bottom contact and practical channel size is desirable. Other issues are reproducibility and durability, which are not described in this article. These issues are important for actual products. Research about the issues will be promoted when organic FETs are really desirable for practical use. When actual production starts and expands, the technology for organic FETs will advance further.

Knowledge of the intrinsic mobility in a pentacene crystal and the upper limit of field-effect mobility for a pentacene FET is important for the physics and device applications. Pentacene TFTs have exhibited high mobilities of more than 1 $cm^2\ V^{-1}\ s^{-1}$, despite their polycrystalline films. This indicates that the intrinsic mobility is higher than those estimated from the characteristics of the TFTs and the further improvement in the mobility of the TFT is possible. Some structural defects with the valley shape exist in a grain, as seen in figure 6 at least. Obtaining pentacene films consisting of grains without such defects leads to improvement in the mobility. Improvement will be also achieved by optimization of the gate insulator surface and reduction of contact resistance. To adjust comprehensively the conditions that influence the mobility will enable the measured mobility to approach the intrinsic mobility.

Acknowledgments

The authors would like to thank Chiang Ooh Tang for pentacene growth and Tadahiro Imada, Daeil Lee and Jong Ho Na for fruitful discussions. This work was supported by the Special Coordination Funds for Promoting Science and Technology.

References

[1] Facchetti A 2007 *Mater. Today* **10** 28–37
[2] Sun Y, Liu Y and Zhu D 2005 *J. Mater. Chem.* **15** 53–65
[3] Katz H E 2004 *Chem. Mater.* **16** 4748–56
[4] The number of papers related to pentacene transistors was obtained by searching with words pentacene and 'transistor(s)' on a database *web of science*
[5] Bailey W J and Madoff M 1953 *J. Am. Chem. Soc.* **20** 5603–4
[6] Clar E and John F 1930 *Berichte der deutschen chemischen gesellschaft* **63** 2967
[7] Horowitz G, Fichou D, Peng X and Garnier F 1991 *Synth. Met.* **41** 1127–30
[8] Dimitrakopoulos C D, Brown A R and Pomp A 1996 *J. Appl. Phys.* **80** 2501–8
[9] Laquindanum J G, Katz H E, Lovinger A J and Dodabalapur A 1996 *Chem. Mater.* **8** 2542–4
[10] Gundlach D J, Lin Y Y, Jackson T N, Nelson S F and Schlom D G 1997 *IEEE Electron Device Lett.* **18** 87–9
[11] Lin Y-Y, Gundlach D J, Nelson S F and Jackson T N 1997 *IEEE Trans. Electron Devices* **44** 1325–31
[12] Lin Y-Y, Gundlach D J, Nelson S F and Jackson T N 1997 *IEEE Electron Device Lett.* **18** 606–8
[13] Klauk H, Halik M, Zschieschang U, Schmid G, Radlik W and Weber W 2002 *J. Appl. Phys.* **92** 5259–63
[14] Kelley T W, Boardman L D, Dunbar T D, Muyres D V, Pellerite M J and Smith T P 2003 *J. Phys. Chem.* B **107** 5877–81
[15] Lee S, Koo B, Shin J, Lee E, Park H and Kim H 2006 *Appl. Phys. Lett.* **88** 162109
[16] Colinge J P, Flandre D and van de Wiele F 1994 *Solid State Electron.* **37** 289

[17] Baccarani G and Ostoja P 1975 *Solid State Electron.* **18** 579–80
[18] Shtein M, Mapel J, Benziger J B and Forrest S R 2002 *Appl. Phys. Lett.* **81** 268–70
[19] Kloc Ch, Simpkins P G, Siegrist T and Laudise R A 1997 *J. Cryst. Growth* **182** 416–27
[20] Laudise R A, Kloc Ch, Simpkins P G and Siegrist T 1998 *J. Cryst. Growth* **187** 449–54
[21] De Kruif C G 1980 *J. Chem. Thermodyn.* **12** 243–8
[22] Oja V and Suuberg E M 1998 *J. Chem. Eng. Data* **43** 486–92
[23] Lee J K, Koo J M, Lee S Y, Choi T Y, Joo J, Kim J-Y and Choi J-H 2002 *Opt. Mater.* **21** 451–4
[24] Blanchet G B, Fincher C R and Malajovich I 2003 *J. Appl. Phys.* **94** 6181–3
[25] Brown A R, Pomp A, de Leeuw D M, Klaassen D B M, Havinga E E, Herwig P and Müllen K 1996 *J. Appl. Phys.* **79** 2136–8
[26] Herwig P T and Müllen K 1999 *Adv. Mater.* **11** 480–3
[27] Afzali A, Dimitrakopoulos C D and Breen T L 2002 *J. Am. Chem. Soc.* **124** 8812–3
[28] Afzali A, Dimitrakopoulos C D and Graham T O 2003 *Adv. Mater.* **15** 2066–9
[29] Weidkamp K P, Afzali A, Tromp R M and Hamers R J 2004 *J. Am. Chem. Soc.* **126** 12740–1
[30] Zander D, Hoffmann N, Lmimouni K, Lenfant S, Petit C and Vuillaume D 2005 *Microelectron. Eng.* **80** 394–7
[31] Afzali A, Kagan C R and Traub G P 2005 *Synth. Met.* **155** 490–4
[32] Uno H, Yamashita Y, Kikuchi M, Watanabe H, Yamada H, Okujima T, Ogawa T and Ono N 2005 *Tetrahedron Lett.* **46** 1981–3
[33] Campbell R B, Robertson J M and Trotter J 1961 *Acta Crystallogr.* **14** 705–11
[34] Minakata T and Natsume Y 2005 *Synth. Met.* **153** 1–4
[35] Butko V Y, Chi X, Lang D V and Ramirez A P 2003 *Appl. Phys. Lett.* **83** 4773–5
[36] Goldmann C, Haas S, Krellner C, Pernstich K P, Gundlach D J and Batlogg B 2004 *J. Appl. Phys.* **96** 2080–6
[37] Reese C, Chung W-J, Ling M, Roberts M and Bao Z 2006 *Appl. Phys. Lett.* **89** 202108
[38] Lee J Y, Roth S and Park Y W 2006 *Appl. Phys. Lett.* **88** 252106
[39] Campbell R B, Robertson J M and Trotter J 1962 *Acta Crystallogr.* **15** 289–90
[40] Farina L, Brillante A, Della Valle R G, Venuti E, Amboage M and Syassen K 2003 *Chem. Phys. Lett.* **375** 490–4
[41] Holmes D, Kumaraswamy S, Matzger A J and Vollhardt K P C 1999 *Chem. Eur. J.* **5** 3399–412
[42] Mattheus C C, Dros A B, Baas J, Meetsma A, de Boer J L and Palstra T T M 2001 *Acta Crystallogr.* C **57** 939–41
[43] Siegrist T, Kloc C, Schön J H, Batlogg B, Haddon R C, Berg S and Thomas G A 2001 *Angew. Chem. Int. Edn* **40** 1732–6
[44] Oehzelt M, Aichholzer A, Resel R, Heimel G, Venuti E and Valle R G D 2006 *Phys. Rev.* B **74** 104103
[45] Mattheus C C, Dros A B, Baas J, Oostergetel G T, Meetsma A, de Boer J L and Palstra T T M 2003 *Synth. Met.* **138** 475–81
[46] Wu J S and Spence J C H 2003 *J. Appl. Crystallogr.* **37** 78–81
[47] Yoshida H and Sato N 2006 *Appl. Phys. Lett.* **89** 101919
[48] Kakudate T, Yoshimoto N and Saito Y 2007 *Appl. Phys. Lett.* **90** 081903
[49] Ruiz R, Mayer A C, Malliaras G G, Nickel B, Scoles G, Kazimirov A, Kim H, Headrick R L and Islam Z 2004 *Appl. Phys. Lett.* **85** 4926–8
[50] Fritz S E, Martin S M, Frisbie C D, Ward M D and Toney M F 2004 *J. Am. Chem. Soc.* **126** 4084–5
[51] Yang H, Shin T J, Ling M-M, Cho K, Ryu C Y and Bao Z 2005 *J. Am. Chem. Soc.* **127** 11542–3
[52] Mattheus C C, de Wijs G A, de Groot R A and Palstra T T M 2003 *J. Am. Chem. Soc.* **125** 6323–30
[53] Doi K, Yoshida K, Nakano H, Tachibana A, Tanabe T, Kojima Y and Okazaki K 2005 *J. Appl. Phys.* **98** 113709
[54] Cornil J, Calbert Ph J and Brédas J L 2001 *J. Am. Chem. Soc.* **123** 1250–1
[55] Cheng Y C, Silbey R J, da Silva Filho D A, Calbert J P, Cornil J and Brédas J L 2003 *J. Chem. Phys.* **118** 3764–74
[56] Troisi A and Orlandi G 2005 *J. Phys. Chem.* B **109** 1849–56
[57] Tiago M L, Northrup J E and Louie S G 2003 *Phys. Rev.* B **67** 115212
[58] Endres R G, Fong C Y, Yang L H, Witte G and Wöll Ch 2004 *Comput. Mater. Sci.* **29** 362–70
[59] Hummer K and Ambrosch-Draxl C 2005 *Phys. Rev.* B **72** 205205
[60] Parisse P, Ottaviano L, Delley B and Picozzi S 2007 *J. Phys.: Condens. Matter* **19** 106209
[61] Hultell M and Stafström S 2006 *Chem. Phys. Lett.* **428** 446–50
[62] Emin D 2000 *Phys. Rev.* B **61** 14543–53
[63] Hannewald K and Bobbert P A 2004 *Phys. Rev.* B **69** 075212
[64] Deng W-Q and Goddard W A 2004 *J. Phys. Chem.* B **108** 8614–21
[65] Pearson G L and Bardeen J 1949 *Phys. Rev.* **75** 865–83
[66] Horowitz G and Hajlaoui M E 2001 *Synth. Met.* **122** 185–9
[67] Di Carlo A, Piacenza F, Bolognesi A, Stadlober B and Maresch 2005 *Appl. Phys. Lett.* **86** 263501
[68] Brown A R, Jarrett C P, de Leeuw D M and Matters M 1997 *Synth. Met.* **88** 37–55
[69] Meijer E J, Matters M, Herwig P T, de Leeuw D M and Klapwijk T M 2000 *Appl. Phys. Lett.* **76** 3433–5
[70] De Angelis F, Cipolloni S, Mariucci L and Fortunato G 2006 *Appl. Phys. Lett.* **88** 193508
[71] Nelson S F, Lin Y-Y, Gundlach D J and Jackson T N 1998 *Appl. Phys. Lett.* **72** 1854–6
[72] Yoneya N, Noda M, Hirai N, Nomoto K, Wada M and Kasahara J 2004 *Appl. Phys. Lett.* **85** 4663–5
[73] Kim W-K and Lee J-L 2007 *Electrochem. Solid-State Lett.* **10** H104–6
[74] Koch N, Kahn A, Ghijsen J, Pireaux J-J, Schwartz J, Johnson R L and Elschner A 2003 *Appl. Phys. Lett.* **82** 70–2
[75] Watkins N J, Yan L and Gao Y 2002 *Appl. Phys. Lett.* **80** 4384–6
[76] Schroeder P G, France C B, Park J B and Parkinson B A 2003 *J. Phys. Chem.* B **107** 2253–61
[77] Ruiz R *et al* 2004 *Chem. Mater.* **16** 4497–508
[78] Tang C O, Kitamura M and Arakawa Y 2004 *Int. Conf. on Solid State Devices and Materials (Tokyo, 2004)* pp 868–9 (F-9-5, extended abstracts)
[79] Stadlober B, Haas U, Maresch H and Haase A 2006 *Phys. Rev.* B **74** 165302
[80] Yagi I, Tsukagoshi K and Aoyagi Y 2004 *Thin Solid Films* **467** 168–71
[81] Tejima M, Kita K, Kyuno K and Toriumi A 2004 *Appl. Phys. Lett.* **85** 3746–8
[82] Yang S Y, Shin K and Park C E 2005 *Adv. Funct. Mater.* **15** 1806–14
[83] Knipp D, Street R A, Völkel A and Ho J 2003 *J. Appl. Phys.* **93** 347–55
[84] Guo D, Ikeda S and Saiki K 2006 *Thin Solid Films* **515** 814–7
[85] Steudel S, De Vusser S, De Jonge S, Janssen D, Verlaak S, Genoe J and Heremans P 2004 *Appl. Phys. Lett.* **85** 4400–2
[86] Lee J, Hwang D K, Choi J-M, Lee K, Kim J H, Im S, Park J H and Kim E 2005 *Appl. Phys. Lett.* **87** 023504
[87] Na J H, Kitamura M, Lee D and Arakawa Y 2007 *Appl. Phys. Lett.* **90** 163514
[88] Sekitani T, Iba S, Kato Y, Noguchi Y and Someya T 2005 *Appl. Phys. Lett.* **87** 173502

[89] Bonfiglio A, Mameli F and Sanna O 2003 *Appl. Phys. Lett.* **82** 3550–2
[90] Pernstich K P, Haas S, Oberhoff D, Goldmann C, Gundlach D J, Batlogg B, Rashid A N and Schitter G 2004 *J. Appl. Phys.* **96** 6431–8
[91] Halik M, Klauk H, Zschieschang U, Schmid G, Dehm C, Schütz M, Maisch S, Effenberger F, Brunnbauer M and Stellacci F 2004 *Nature* **431** 963–6
[92] Kobayashi S, Nishikawa T, Takenobu T, Mori S, Shimoda T, Mitani T, Shimotani H, Yoshimoto N, Ogawa S and Iwasa Y 2004 *Nat. Mater.* **3** 317–22
[93] Klauk H, Zschieschang U, Pflaum J and Halik M 2007 *Nature* **445** 745–8
[94] Yagi I, Tsukagoshi K and Aoyagi Y 2005 *Appl. Phys. Lett.* **86** 103502
[95] Yaginuma S, Yamaguchi J, Itaka K and Koinuma H 2005 *Thin Solid Films* **486** 218–21
[96] Fujisaki Y, Inoue Y, Kurita T, Tokito S, Fujikake H and Kikuchi H 2004 *Japan. J. Appl. Phys.* **43** 372–7
[97] Majewski L A, Schroeder R and Grell M 2005 *Adv. Funct. Mater.* **15** 1017–22
[98] Kitamura M and Arakawa Y 2006 *Appl. Phys. Lett.* **89** 223525
[99] Peacock P W and Robertson J 2002 *J. Appl. Phys.* **92** 4712–21
[100] Jang Y, Kim D H, Park Y D, Cho J H, Hwang M and Cho K 2006 *Appl. Phys. Lett.* **88** 072101
[101] Kato Y, Iba S, Teramoto R, Sekitani T, Someya T, Kawaguchi H and Sakurai T 2004 *Appl. Phys. Lett.* **84** 3789–91
[102] Stadlober B, Zirkl M, Beutl M, Leising G, Bauer-Gogonea S and Bauer S 2005 *Appl. Phys. Lett.* **86** 242902
[103] De Angelis F, Cipolloni S, Mariucci L and Fortunato G 2005 *Appl. Phys. Lett.* **86** 203505
[104] Chou W-Y, Kuo C-W, Cheng H-L, Chen Y-R, Tang F-C, Yang F-Y, Shu D-Y and Liao C-C 2006 *Appl. Phys. Lett.* **89** 112126
[105] Deman A L and Tardy J 2006 *Mater. Sci. Eng.* C **26** 421–6
[106] Hwang D K, Lee K, Kim J H, Im S, Kim C S, Baik H K, Park J H and Kim E 2006 *Appl. Phys. Lett.* **88** 243513
[107] Park J, Kang S I, Jang S P and Choi J S 2005 *Japan. J. Appl. Phys.* **44** 648–51
[108] Chu C-W, Li S-H, Chen C-W, Shrotriya V and Yang Y 2005 *Appl. Phys. Lett.* **87** 193508
[109] Chen F-C, Kung L-J, Chen T-H and Lin Y-S 2007 *Appl. Phys. Lett.* **90** 073504
[110] Gundlach D J, Jia L L and Jackson T N 2001 *IEEE Electron Device Lett.* **22** 571–3
[111] Kim W-K and Lee J-L 2006 *Appl. Phys. Lett.* **88** 262102
[112] Yoneya N, Noda M, Hirai N, Nomoto K, Wada M and Kasahara J 2004 *Appl. Phys. Lett.* **85** 4663
[113] Mach P, Rodriguez S J, Nortrup R, Wiltzius P and Rogers J A 2001 *Appl. Phys. Lett.* **78** 3592–4
[114] Sheraw C D *et al* 2002 *Appl. Phys. Lett.* **80** 1088–90
[115] Nomoto K, Hirai N, Yoneya N, Kawashima N, Noda M, Wada M and Kasahara J 2005 *IEEE Trans. Electron Devices* **52** 1519–26
[116] Kawasaki M, Imazeki S, Ando M, Sekiguchi Y, Hirota S, Umemura S and Kamata T 2006 *IEEE Trans. Electron Devices* **53** 435–41
[117] Kitamura M, Imada T and Arakawa Y 2003 *Appl. Phys. Lett.* **83** 3410–2
[118] Kitamura M, Imada T and Arakawa Y 2003 *Japan. J. Appl. Phys.* **42** 2483–7
[119] Ohta S, Chuman T, Miyaguchi S, Satoh H, Tanabe T, Okuda Y and Tsuchida M 2005 *Japan. J. Appl. Phys.* **44** 3678–81
[120] Zhou L, Park S, Bai B, Sun J, Wu S-C, Jackson T N, Nelson S, Freeman D and Hong Y 2005 *IEEE Electron Device Lett.* **26** 640–2
[121] Zhou L, Wanga A, Wu S-C, Sun J, Park S and Jackson T N 2006 *Appl. Phys. Lett.* **88** 083502
[122] Mizukami M *et al* 2006 *IEEE Electron Device Lett.* **27** 249–51
[123] Ando S, Murakami R, Nishida J, Tada H, Inoue Y, Tokito S and Yamashita Y 2005 *J. Am. Chem. Soc.* **127** 14996–7
[124] Tatemichi S, Ichikawa M, Koyama T and Taniguchi Y 2006 *Appl. Phys. Lett.* **89** 112108
[125] Anthopoulos T D, Singh B, Marjanovic N, Sariciftci N S, Ramil A M, Sitter H, Cölle M and de Leeuw D M 2006 *Appl. Phys. Lett.* **89** 213504
[126] Kitamura M and Arakawa Y 2007 *Appl. Phys. Lett.* **91** 053505
[127] Ahles M, Schmechel R and von Seggern H 2005 *Appl. Phys. Lett.* **87** 113505
[128] Kang S J, Yi Y, Kim C Y, Cho K, Seo J H, Noh M, Jeong K, Yoo K-H and Whang C N 2005 *Appl. Phys. Lett.* **87** 233502
[129] Singh Th B, Senkarabacak P, Sariciftci N S, Tanda A, Lackner C, Hagelauer R and Horowitz G 2006 *Appl. Phys. Lett.* **89** 033512